

# Diffractive oblique plane microscopy: supplementary material

**MAXIMILIAN HOFFMANN AND BENJAMIN JUDKEWITZ\***

Charité Universitätsmedizin Berlin, Einstein Center for Neuroscience, NeuroCure Cluster of Excellence, Berlin, Germany, Charitéplatz 1, 10117 Berlin, Germany

\*Corresponding author: [benjamin.judkewitz@charite.de](mailto:benjamin.judkewitz@charite.de)

10.1002/oeq.1000

---

This document provides supplementary information to "Diffractive oblique plane microscopy," <https://doi.org/10.1364/optica.6.001166>.

---

## 1. SHEAR TRANSFORMATION

Prior to all data analysis the data was transformed to the rectangular lab coordinate system from its native sheared geometry (s. Figure 1c), via the 3d affine transformation

$$A = \begin{pmatrix} 1 & 0 & 0 & 0 \\ 0 & 1 & -\tan(\theta) & 0 \\ 0 & 0 & \cos(\theta) & 0 \\ 0 & 0 & 0 & 1 \end{pmatrix}$$

(homogeneous coordinates, scale and shear), where  $\theta$  is the grating angle with respect to the optical axis. This was done either by `imwarp` (Matlab, Mathworks Inc., linear interpolation) or `warpAffine` (opencv 3, linear interpolation).

## 2. IMAGING OF BEADS AND QUANTIFICATION OF RESOLUTION

Fluorescent beads (diameter  $1 \mu\text{m}$ ) were dispersed in a polyacrylamide gel between a coverslide and a coverslip held apart by a silicon spacer. A stack of the whole accessible image volume at an isotropic voxel size of  $1.625 \mu\text{m}$  was taken. The stack was then transformed as described in section A. The stack was thresholded at the 99.99th percentile and all connected components were segmented out within a ROI of  $33 \times 33 \times 303 \mu\text{m}$  ( $X \times Y \times Z$ ). For the quantification of the lateral resolution each ROI was maximum intensity projected along  $z$ . The lateral resolution in  $x$  and  $y$  were determined as the fullwidth-half maximum (FWHM) of the line plot through the maximum of this projection. The axial sectioning capability was determined as the FWHM of the sum of all pixel values along the  $XY$  planes of each bead volume. Often two or more beads were axially contained in one ROI, which manifested in a bimodal distribution of the axial sectioning FWHM. This bi-modal distribution was fit by a Gaussian mixture model. The ROIs belonging to the distribution with the higher mean and therefore contained multiple beads were excluded from the analysis.

## 3. IMAGING OF ZEBRAFISH LARVA

A Zebrafish larva 4 days post fertilization (dpf) (elav13:H2B-GCaMP6s) was restrained by embedding it in agarose (2% Low melting point) and placed under the microscope. All images were taken with 3 ms exposure time, a 2 ms lasersweep time and an average laser power of 11mW at the image plane.

## 4. IMAGING OF JUVENILE ZEBRAFISH

A juvenile Zebrafish larva 33 dpf (elav13:H2B-GCaMP6s) was restrained by embedding it in agarose (2% Low melting point) and placed under the microscope. All images were taken with 3 ms exposure time, a 2 ms lasersweep time and an average laser power of 11mW at the image plane.

## 5. ROI EXTRACTION

The extraction of fluorescence traces and spatial footprints from single cells was done by performing the cell segmentation of the `CaImAn` package [5, 6] on subblocks of the imaging data with greedyROI initialisation. The footprints and traces were then aggregated and only ROIs with a standard deviation above the 70.1th percentile were kept. This threshold was chosen, as it was seen to reject spurious and noisy ROIs by manual inspection.  $\Delta F/F$  traces were calculated by subtracting and dividing each extracted trace by its temporal mean.

## 6. COMPARISON WITH PREVIOUS OBLIQUE PLANE MICROSCOPY TECHNIQUES

Compared to other OPM techniques, DOPM trades off photon efficiency and resolution for field of view (FOV). This trade-off is not unique to DOPM, but reflects a general inverse scaling between FOV and numerical aperture (NA). [7]

**Table S1.** Comparison of performance parameters of the DOPM with recent OPM publications

Parameter	DOPM	SCAPE[1]	SOPi(1P)[2][3]
Reported Lateral Resolution	$2.6 \mu\text{m} \times 3.1 \mu\text{m}$	$2.5 \mu\text{m} \times 3.25 \mu\text{m}$	$1.30 \mu\text{m}$
Reported Axial Resolution	$37.4 \mu\text{m}$	$3.6 \mu\text{m}$	unspecified
Max. Field Of View	$3.3 \times 3.0 \times 1.0 \text{ mm}^3$	$600 \times 1000 \times 550 \mu\text{m}^3$	$850 \times 325 \times 500 \mu\text{m}^3$
Resolvable Image Points (FOV/Resolution)	$\approx 3.5 \cdot 10^7$	$\approx 1.1 \cdot 10^7$	-

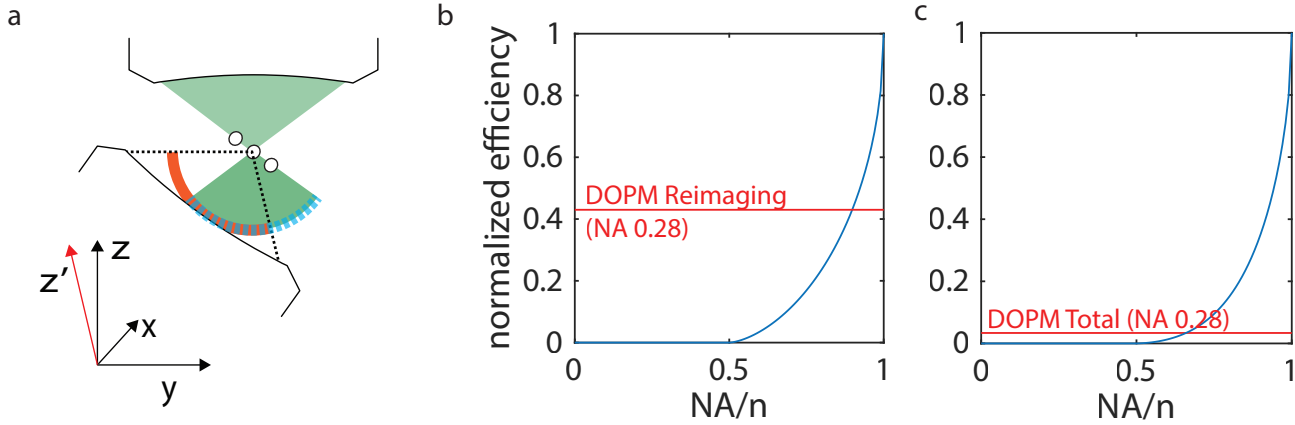


**Fig. S1.** DOPM and OPM efficiency: a) As depicted here and in Figure 1a the conventional reimaging step of the oblique plane microscopy leads to loss of light. A part of the light cone emerging from the first objective is not collected because it does not propagate within the acceptance angle of the second objective. The percentage of light that is retained can be approximated by the area of the intersection of two spherical caps (red, dashed blue). [4] Here we always assume that the oblique plane is at the maximally permitted angle. b) The resulting efficiency of the reimaging step is plotted for different numerical apertures (NA). The efficiency of the diffractive reimaging step in our setup is marked by a red line and intersects the curve at  $NA = 0.9$ . However it is only possible up to an NA of 0.71 due to geometrical constraints c) The theoretical total throughput of OPM for different NAs. Because the total light collection efficiency scales with the  $NA^2$  our low-NA system captures less light than higher NA systems, even though our reimaging step is not necessarily less efficient.

Here we decided to use an object side NA of 0.28 and not 1.0 as previous publications [1–3] to achieve an imaging volume which is  $\sim 30\times$  larger than previous volumes achieved with OPM. [1].

The low NA leads to a decreased resolution compared to previous techniques. This effect is most pronounced in the axial direction, where the resolution scales as  $NA^2$  and the sectioning capability is determined by the angle of the imaging plane with respect to the optical axis. At the same time DOPM features a larger imaging volume and therefore delivers as many resolvable image points as previous techniques. (s. Table S1)

The low numerical aperture of our system also reduces the optical throughput by a factor  $1/NA^2 = 1/0.28^2 \approx 12$  in comparison to previous techniques.

In addition, the reimaging geometry of oblique plane microscopes leads to a loss of light. However a comparison between the conventional OPM (s. Figure S1) and the diffractive solution reveals that the efficiency of the diffractive solution at  $NA/n = 0.28$  is, where geometrically possible (up to  $NA/n = 0.71$ ), higher than the one of previous OPMs ( $NA/n = 0.75$ ). Therefore it might be advantageous to use the diffractive solution to reimaging even above  $NA = 0.5$ , where it is not strictly necessary to achieve oblique reimaging.

## 7. DISPERSION AND MULTICOLOR IMAGING

As stated in the main text the diffraction grating does not lead to additional chromatic aberrations because its surface is directly imaged onto a camera, where different wavelengths are again combined. This however is subject to the condition that the diffracted light is propagating within the acceptance cone of the third objective. Because the grating is a dispersive element light of different wavelengths will be diffracted into different directions and could in principle be diffracted outside of the acceptance cone. Whether this is the case can be calculated with the grating equation

$$(m\lambda/d - \sin(\alpha)) = \sin(\beta)$$

In our case  $\alpha = (90 - 14.6)^\circ$  is the incidence angle and  $\beta$  is the diffraction angle with respect to the grating normal,  $d = 555 \text{ nm}$  is the grating period, and  $m$  is an integer. According to this formula for our system all light that lies in between 380 and 694 nm, which includes most fluorophores used in biology, will still be imaged without any clipping. (s. Figure S2)

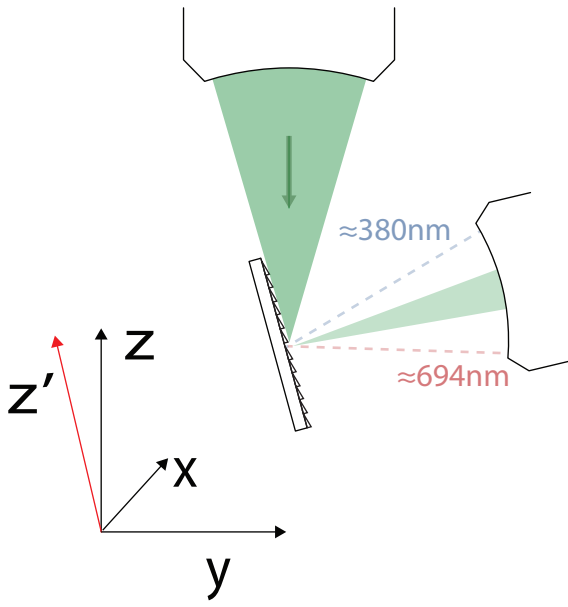


**Fig. S2.** The reimaging step at the grating is depicted. The numerical aperture of the incoming beam is diminished along one direction due to diffraction at the grating. After the grating light of different wavelength travels in different direction, but in our system with NA=0.28 all light between 380 nm and 694 nm would be collected.

## REFERENCES

1. M. B. Bouchard, V. Voleti, C. S. Mendes, C. Lacefield, W. B. Grueber, R. S. Mann, R. M. Bruno, and E. M. C. Hillman, "Swept confocally-aligned planar excitation (SCAPE) microscopy for high-speed volumetric imaging of behaving organisms," *Nat. Photonics* **9**, 113–119 (2015).
2. M. Kumar and Y. Kozorovitskiy, "Tilt-invariant scanned oblique plane illumination microscopy for large-scale volumetric imaging," *Opt. Lett.* **44**, 1706–4 (2019).
3. M. Kumar, S. Kishore, J. Nasenbeny, D. L. McLean, and Y. Kozorovitskiy, "Integrated one-and two-photon scanned oblique plane illumination (sopi) microscopy for rapid volumetric imaging," *Opt. express* **26**, 13027–13041 (2018).
4. Y. Lee and W. C. Kim, "Concise formulas for the surface area of the intersection of two hyperspherical caps," KAIST Tech. Rep. (2014).
5. E. A. Pnevmatikakis, Y. Gao, D. Soudry, D. Pfau, C. Lacefield, K. Poskanzer, R. Bruno, R. Yuste, and L. Paninski, "A structured matrix factorization framework for large scale calcium imaging data analysis," arXiv preprint arXiv:1409.2903 (2014).
6. A. Giovannucci, J. Friedrich, P. Gunn, J. Kalfon, B. L. Brown, S. A. Koay, J. Taxidis, F. Najafi, J. L. Gauthier, P. Zhou, B. S. Khakh, D. W. Tank, D. B. Chklovskii, and E. A. Pnevmatikakis, "CaImAn an open source tool for scalable calcium imaging data analysis," *eLife* **8**, 413 (2019).
7. A. W. Lohmann, "Scaling laws for lens systems." *Appl. Opt.* **28**, 4996–4998 (1989).